that the particular rendering of folded EPO **1**, shown in Fig. 4, is provided for convenience solely by analogy with a reported structure of a tri-Lys24,38,83-mutated EPO aglycone bound to the EPO receptor (*34*).

The ability to reach a molecule of the complexity of **1** by entirely chemical means provides convincing testimony about the growing power of organic synthesis. As a result of synergistic contributions from many laboratories, the aspirations of synthesis may now include, with some degree of realism, structures hitherto referred to as "biologics"— a term used to suggest accessibility only by biological means (isolation from plants, fungi, soil samples, corals, or microorganisms, or by recombinant expression). Formidable as these methods are for the discovery, development, and manufacturing of biologics, one can foresee increasing needs and opportunities for chemical synthesis to provide the first samples of homogeneous biologics. As to production, the experiments described above must be seen as very early days. In no way do we mean to suggest that chemical synthesis is competitive with biologic-type methods to produce EPO, if product homogeneity is not of concern. However, one can well imagine that with continuing improvements in the practicality of solid-phase peptide synthesis (*35*, *36*), new ligation methods, the operational handling of synthetic polypeptides, and enzymatic means of oligosaccharide assembly, synthesis is likely to be of growing value, even in terrains currently described as strictly biologic (*39*).

### References and Notes

1. S. Elliott, M. A. Foote, G. Molineux, *Erythropoietins, Erythropoietic Factors, and Erythropoiesis* (Birkhäuser, Basel, Switzerland, ed. 2, 2009).
2. A. J. Sytkowski, *Erythropoietin* (Wiley-VCH, Weinheim, Germany, 2004).
3. R. S. Rush *et al.*, *Anal. Chem.* **67**, 1442–1452 (1995).
4. P. Wang *et al.*, *Angew. Chem. Int. Ed.* **51**, 11576–11584 (2012).
5. R. M. Wilson, S. Dong, P. Wang, S. J. Danishefsky, *Angew. Chem. Int. Chem.* **52**, 7646–7665 (2013).
6. During the course of these investigations, ongoing studies from other laboratories provided striking results in reaching congeners of various sorts with promising erythropoietic activity. This work is summarized in (*5*) and includes references (*31*, *37*, *38*).
7. B. Wu *et al.*, *Tetrahedron Lett.* **47**, 5577–5579 (2006).
8. B. Wu *et al.*, *Tetrahedron Lett.* **47**, 8009–8011 (2006).
9. S. J. Danishefsky, M. T. Bilodeau, *Angew. Chem. Int. Ed. Engl.* **35**, 1380–1419 (1996).
10. S. J. Danishefsky, J. R. Allen, *Angew. Chem. Int. Ed.* **39**, 836–863 (2000).
11. J. B. Schwarz *et al.*, *J. Am. Chem. Soc.* **121**, 2662–2673 (1999).
12. There are over 50 glycoforms of recombinant EPO containing combinations of bi-, tri-, and tetraantennary carbohydrate domains, which have not been separated or fully characterized [see (*13*)].
13. H. Sasaki, B. Bothner, A. Dell, M. Fukuda, *J. Biol. Chem.* **262**, 12059–12076 (1987).
14. M. Takeuchi, A. Kobata, *Glycobiology* **1**, 337–346 (1991).
15. S. R. Hamilton *et al.*, *Science* **313**, 1441–1443 (2006).
16. J. H. Nett *et al.*, *J. Biotechnol.* **157**, 198–206 (2012).
17. P. E. Dawson, T. W. Muir, I. Clark-Lewis, S. B. Kent, *Science* **266**, 776–779 (1994).
18. Q. Wan, S. J. Danishefsky, *Angew. Chem. Int. Ed.* **46**, 9248–9252 (2007).
19. L. Z. Yan, P. E. Dawson, *J. Am. Chem. Soc.* **123**, 526–533 (2001).
20. J. D. Warren, J. S. Miller, S. J. Keding, S. J. Danishefsky, *J. Am. Chem. Soc.* **126**, 6576–6578 (2004).
21. G. Chen *et al.*, *J. Am. Chem. Soc.* **128**, 7460–7462 (2006).
22. S. Dong, S. Shang, Z. Tan, S. J. Danishefsky, *Isr. J. Chem.* **51**, 968–976 (2011).
23. P. Wang, B. Aussedat, Y. Vohra, S. J. Danishefsky, *Angew. Chem. Int. Ed.* **51**, 11571–11575 (2012).
24. V. Ullmann *et al.*, *Angew. Chem. Int. Ed.* **51**, 11566–11570 (2012).
25. D. Bang, S. B. Kent, *Angew. Chem. Int. Ed.* **43**, 2534–2538 (2004).
26. S. Sakakibara, *Biopolymers* **37**, 17–28 (1995).
27. S. Liu, B. L. Pentelute, S. B. Kent, *Angew. Chem. Int. Ed.* **51**, 993–999 (2012).
28. The mass spectrum of **10** (figs. S24 and S25) is supportive of the assignment. However, as is the case with previous attempts at obtaining high-quality readouts from extensively glycosylated polysialic acid-containing domains, this attempt has not been fully successful.
29. E. Llop, R. Gutiérrez-Gallego, J. Segura, J. Mallorquí, J. A. Pascual, *Anal. Biochem.* **383**, 243–254 (2008).
30. V. P. Saxena, D. B. Wetlaufer, *Biochemistry* **9**, 5015–5023 (1970).
31. G. G. Kochendoerfer *et al.*, *Science* **299**, 884–887 (2003).
32. L. O. Narhi *et al.*, *Protein Eng.* **14**, 135–140 (2001).
33. M. A. Recny, H. A. Scoble, Y. Kim, *J. Biol. Chem.* **262**, 17156–17163 (1987).
34. R. S. Syed *et al.*, *Nature* **395**, 511–516 (1998).
35. R. B. Merrifield, *J. Am. Chem. Soc.* **85**, 2149–2154 (1963).
36. T. Wang, S. J. Danishefsky, *Proc. Natl. Acad. Sci. U.S.A.* **110**, 11708–11713 (2013).
37. K. Hirano, D. Macmillan, K. Tezuka, T. Tsuji, Y. Kajihara, *Angew. Chem. Int. Ed. Engl.* **48**, 9557–9560 (2009).
38. M. Murakami, R. Okamoto, M. Izumi, Y. Kajihara, *Angew. Chem. Int. Ed. Engl.* **51**, 3567–3572 (2012).
39. Information on materials and methods, including spectroscopic data of new compounds, is available on *Science* Online.

# The Missing Mountain Water: Slower Westerlies Decrease Orographic Enhancement in the Pacific Northwest USA

C. H. Luce,[1]* J. T. Abatzoglou,[2] Z. A. Holden[3]

Trends in streamflow timing and volume in the Pacific Northwest United States have been attributed to increased temperatures, because trends in precipitation at lower-elevation stations were negligible. We demonstrate that observed streamflow declines are probably associated with declines in mountain precipitation, revealing previously unexplored differential trends. Lower-troposphere winter (November to March) westerlies are strongly correlated with high-elevation precipitation but weakly correlated with low-elevation precipitation. Decreases in lower-tropospheric winter westerlies across the region from 1950 to 2012 are hypothesized to have reduced orographic precipitation enhancement, yielding differential trends in precipitation across elevations and contributing to the decline in annual streamflow. Climate projections show weakened lower-troposphere zonal flow across the region under enhanced greenhouse forcing, highlighting an additional stressor that is relevant for climate change impacts on hydrology.

Despite the importance of mountains as sources of water and the conservation of biodiversity, particularly in a changing climate, our understanding of climate change in them is limited because of sparse observational data and difficult modeling conditions (*1*). Although the consequences of increased temperature for mountain snow are relatively well understood and severe (*2*–*4*), poor information about both historical and projected changes in mountain precipitation may lead to substantial misjudgment of risks and maladaptation. In particular, ecosystems and water supplies may be more sensitive to declines in precipitation than to increases in temperature (*5*–*7*).

We synthesized across multiple data sources to infer substantial historical declines in precipitation in the Cascades and Northern Rockies of the Pacific Northwest (PNW) United States and linked them to observed changes in atmospheric circulation. These historical declines contradict published assessments that there have probably been no significant declines in PNW precipitation over the past 60 years (*4*, *8*, *9*). The information basis for the lack of historical decline is the estimation of trends from the U.S. Historical Climate Network (HCN) precipitation stations in the PNW

[1]U.S. Forest Service Research and Development, 322 East Front Street, Boise, ID 83702, USA. [2]Department of Geography, University of Idaho, 875 Perimeter Drive, Moscow, ID 83844, USA. [3]U.S. Forest Service Region 1, 200 East Broadway Street, Missoula, MT 59807, USA.

*Corresponding author. E-mail: cluce@fs.fed.us

showing mostly nonsignificant declines in precipitation over the region from 1948 to 2006 (Fig. 1). In contrast, annual (by water year) streamflows from relatively undisturbed watersheds in the PNW have shown marked declines (*10–12*).

One hypothesis for the cause of declining trends in streamflow is increased evapotranspiration (ET). Because very few of the HCN precipitation stations fall within the watersheds where streamflow was measured (Fig. 1), direct assessment of the water balance through comparison of precipitation and streamflow in the basins would have substantial uncertainty. However, the energy balance provides an important limiting condition.

Closure of the energy balance in a warming environment requires that increases in ET not exceed increased external energy input (such as downwelling longwave radiation). This sets an upper limit on ET, forming a robust test of whether ET could explain flow trends. Trends in downwelling longwave and shortwave radiation from NCEP/NCAR (National Centers for Environmental Prediction/National Center for Atmospheric Research) Reanalysis 1 over the region do not have a significant trend, although the global average increase in radiative forcing over the late 20th century is ~1.6 W/m$^2$ (confidence range 0.6 to 2.4 W/m$^2$) (*1*). The decline in flow per unit of area of watershed multiplied by the latent heat of vaporization gives an estimate of the energy cost if all streamflow losses are assumed to result from ET (averaged here across the entire year). In all but the driest basins, the energy requirement to explain the observed historical trend in the 25th-percentile flows exceeds the increase in downwelling long-

wave radiation (fig. S2), in some cases by an order of magnitude. We can further augment the available energy by considering increases in net radiation due to earlier snowmelt (earlier loss in albedo), but would still see only a marginal increase of ~2.9 W/m$^2$ for the annual average per week of advance (supplementary materials), which would still not explain the magnitude of observed streamflow changes.

The disparity between declining streamflows that cannot be explained by ET and insignificant trends at precipitation stations presents an important but previously unrecognized paradox. Stream gauges integrate precipitation across elevation gradients in mountain basins, whereas HCN precipitation stations primarily sample low elevations (Fig. 1 and fig. S3). The substantial declines in annual flow thus imply differential trends in high- and low-elevation precipitation.

Orographic enhancement of precipitation is a primary driver of the geographic distribution of precipitation across the PNW and other mountainous regions (*13*). A majority of the precipitation received in the PNW occurs during October to April, when a progressive storm track and embedded cyclones advect moist and stably stratified air masses toward mountain barriers, thereby providing conditions conducive to upslope precipitation enhancement. To underscore the broad importance of orographic precipitation enhancement in the region, the average annual precipitation from the HCN is 712 mm, whereas the average annual streamflow at the 43 gauges (which do not account for ET) is 1063 mm.

A fundamental dynamic driver of orographic enhancement is the lower-tropospheric wind speed

normal to a mountain barrier (*14–17*), which has been shown to explain a substantial proportion of interstorm and interannual variability in orographic enhancement (*18–22*). Westerly lower-tropospheric flow is hypothesized to modulate orographic precipitation enhancement, because major mountain ranges of the PNW are broadly N-S oriented. Correlations between regionally averaged (42.5° to 47.5°N, 115° to 130°W) November-March lower-tropospheric westerly wind speeds at 700 hPa (u700) and November-March precipitation at higher-elevation Snowpack Telemetry (SNOTEL) stations was stronger than at lower-elevation HCN stations (Fig. 2 and fig. S6). Orographic precipitation enhancement is strongest on the windward sides of mountain barriers and a short distance leeward of the crest. Blocking, a phenomenon in which some air stagnates near the base of steep mountain barriers, can extend the mountain front influence upwind (*23*). These same patterns are visible in correlations between precipitation and u700 in transects across the region (Fig. 2). At a regional scale, orographic precipitation enhancement is not strictly elevation-related; rather, the effect is related to proximity to strong elevation gradients. Some stations of the HCN network sample "low-elevation" areas with orographic precipitation enhancement, although few have strong correlations (fig. S6), and the great majority of HCN stations are not in places that are usually associated with orographic enhancement. Correlations between annual streamflow and u700 are about the same strength as in the SNOTEL data (fig. S6).

u700 declined over the period from 1950 to 2012 (Fig. 3), with a more pronounced trend in lower extremes (0.3 m/s/decade, $P = 0.015$) than the mean (0.2 m/s/decade, $P = 0.034$), similar in pattern to streamflow trends. Others have also reported declines in u700 over this period in other regions (*24, 25*). A portion of the interannual variability in u700 is linearly correlated with large-scale modes of climate variability realized through the El Niño–Southern Oscillation [correlation coefficient ($r^2$) = 0.28, $P < 0.001$], the Pacific Decadal Oscillation ($r^2 = 0.33$, $P < 0.001$), and the Pacific North American pattern ($r^2 = 0.3$, $P < 0.001$). Together they explain some ($r^2 = 0.37$, $P = <0.001$) but not a majority of the interannual variability, and decreases in u700 persist when the influence of these climate modes is linearly removed (fig. S4). This supports an argument that factors exogenous to primary modes of internal climate variability may be associated with observed u700 decreases.

Changes in u700 might be expected with differential warming rates associated with latitude and land-ocean contrasts through their effect on midlatitude meridional thermal gradients (MTGs, the N-S gradient in temperature) (*26*). Historically, interannual variations in u700 over the PNW have been associated with the regional MTG ($r^2 = 0.73$, fig. S8). When 20th-century trends in the Coupled Model Intercomparison Project Phase 5 (CMIP5) were examined, 16 of the 24 models
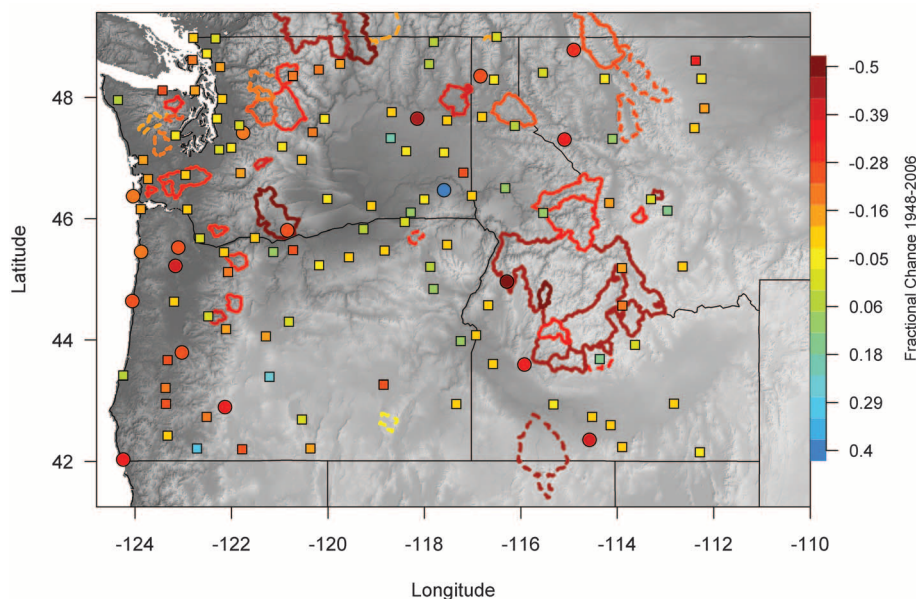


**Fig. 1. Location and trends of lower-quartile annual (water-year) precipitation and streamflow at HCN precipitation stations (points) and Hydro-Climatic Data Network streamflow gauges (watershed outlines) from 1948 to 2006.** Statistically significant trends are denoted with circles for precipitation and with solid boundaries for streamflow. Squares and dashed boundaries denote nonsignificant trends.

polled showed a negative trend in u700, with historical radiative forcing having a median trend of –0.2 m/s over the 1950–2005 simulated period (20% of the trend in Fig. 3 and table S1), and comparison of future differences in u700 assessed from these models between 2071–2100 and 1950–2005 for experiment RCP8.5 show a small, yet systematic decline during the winter on the order of 0.65 m/s (6.5%) for the region addressed in this study (Fig. 4 and table S1). The regional slowing of the lower-tropospheric westerlies may be partially a consequence of a general relaxation of the regional MTG associated with differential rates of winter warming across the broader region (fig. S9). The average projected change in u700 over the 21st century is only slightly greater than the observed decrease, and both represent a substantial decline with respect to the 1950–2005 average (fig. S3). Both the past two decades and projected mean wind speed represent dry conditions for the PNW, with current streamflows being comparable to the 1930s, recognized regionally as one of the driest periods in the past few centuries [(27–29) and supplementary materials].

The slopes of the regressions between SNOTEL precipitation and u700 were on the order of 10 to 15% of precipitation per unit (1 m/s) of change in u700 (fig. S6) and broadly show the same geographic pattern as the correlations (fig. S5). Decline in the mean u700 over the period was about 1 m/s, and these slopes are comparable to the average decline in mean streamflow of 16% over the period (10). Some of the difference between observed and modeled decline may be due to changes in atmospheric moisture fluxes related to water vapor content changes that also contribute to orographic enhancement (30). Long-term changes in moisture availability and temperature are likely to modulate the influence of wind changes on orographic precipitation enhancement, but the mechanisms are varied and complex and rely on assumptions about upwind boundary conditions and cloud microphysics, making projections uncertain and requiring more complex modeling efforts (17, 31).

The topography used by global circulation models (GCMs) substantially flattens even the largest mountain ranges, minimizing their influence on air masses and precipitation. Although GCMs capture the effects of the broadening Hadley cell and poleward movement of midlatitude storm tracks, yielding general agreement on decreased precipitation and streamflow in the southwestern U.S. (32), the effects of decreased midlatitude westerly wind speeds on orographic precipitation have not been accounted for in mountainous regions. Regional climate models (RCMs) that better resolve mountain ranges could conceptually help frame expectations regarding orographic precipitation (33). However, parameterizations of fine-scale processes still require tuning to empirical observations, and information about high-elevation precipitation trends implicit in streamflow data may assist with calibration.

Better precipitation projections for mountainous areas are critical because of (i) their importance for the conservation of biodiversity in a changing climate, and (ii) their importance as a water supply for downstream agriculture, industry, energy, and municipal use. Although mountains may serve as refugia for cold-adapted species and reservoirs for late-season runoff, decreases in high-elevation precipitation combined with warming temperatures and shifts in precipitation phases could have profound consequences for the ecohydrology of mountain ecosystems. Decreases in precipitation, particularly in the driest years, increase the risk of forest fires and may pose a greater risk than temperature increases (5), although more broadly combined drying and warming are most detrimental (34). Cold-water aquatic species faced with warm-

ing stream temperatures will seek higher elevations and smaller tributary streams (35) but may find less habitat there as headwater streamflows decrease.

Previous studies have attributed changes in streamflow timing, spring onset, and snowpack to warming temperatures (2, 4, 36). Our findings suggest that an additional mechanism—decreased orographic precipitation enhancement associated with decreases in zonal winds—may also have contributed to observed trends. The lack of concordance between the traditionally used HCN network and either higher-elevation SNOTEL stations or streamflow measurements should place an important caveat on the assumption that circulation and precipitation have been unaffected in this region, particularly in the mountains, where most precipitation falls.
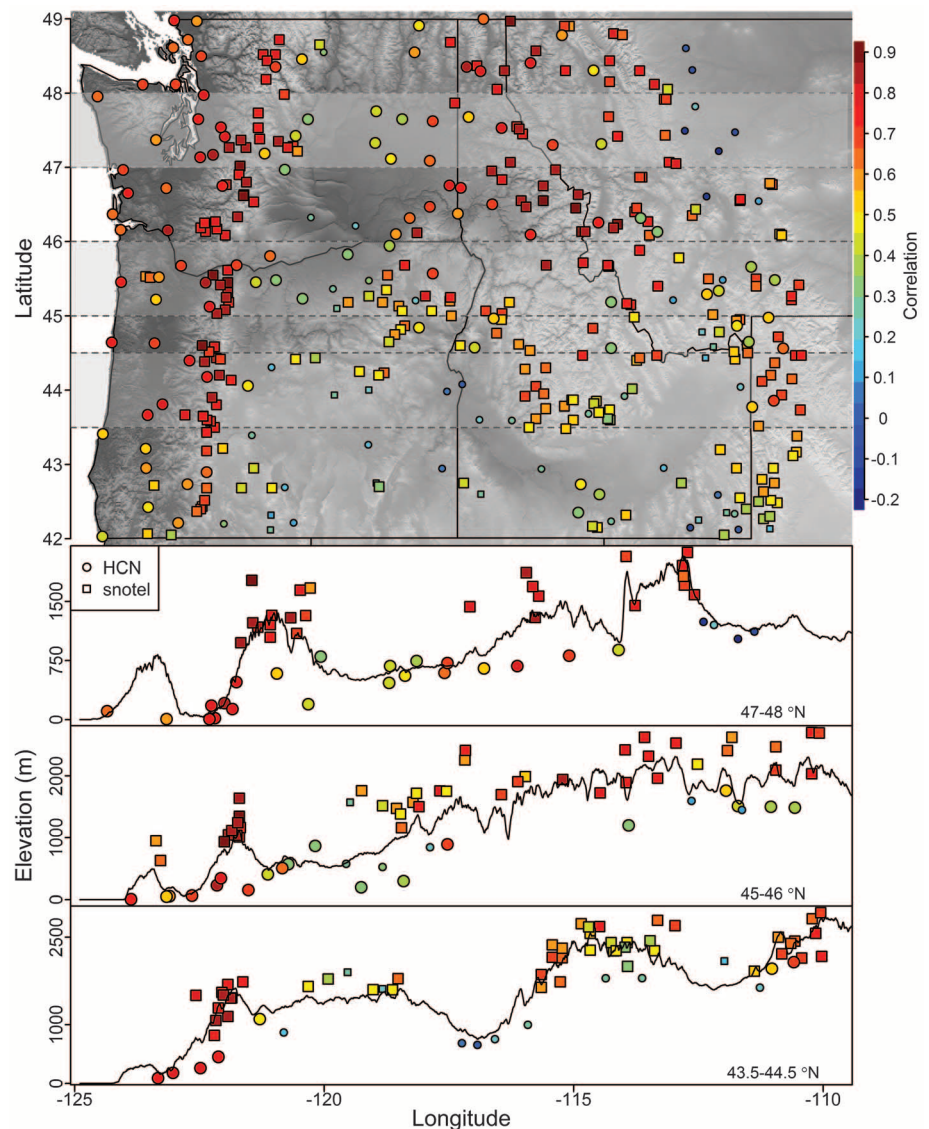
**Fig. 2. Correlation of 1982–2012 November to March HCN (circles) and SNOTEL (squares) precipitation with November to March u700 zonal winds over 42.5° to 47.5°N and 115° to 130°W.** Three longitudinal transects (lower panels) show examples of the pattern of correlations with elevation. The larger symbols indicate statistical significance (P < 10%).

Improved understanding of the relative roles of temperature and precipitation on snowpack storage and runoff timing is critical for climate change adaptation. One of the recommendations for adaptation to earlier snowmelt is to increase the storage capacity in reservoirs to replace snowpack storage; however, in circumstances of declining precipitation, this could be maladaptive. For instance, reductions in snowpack storage driven by reduced precipitation would also result in earlier streamflow timing (5, 10). In such a case, a dam would represent another consumptive use of water, and the water rights necessary to fill the dam may not be available in the driest and consequently "earliest" years.

The lack of long-term precipitation data from mountains severely limits our understanding of historical trends and the empirical framework needed for understanding impacts of climate variability and change. The analyses here further highlight the importance of historical streamflow and wind data and suggest that they could be used to extend high-elevation precipitation records to earlier periods or enhance existing gridded historical climatological data sets. Interannual variability in orographic enhancement is partially captured by the SNOTEL network, dating to the 1980s. However, reliance on time-invariant orographic precipitation ratios for earlier

historical analyses may lead to errors in interpreting trends, because the differential changes in low-elevation and high-elevation precipitation are not reflected.

Prediction of orographic precipitation effects in a changing climate has been acknowledged as a difficult task that depends on a number of assumptions (17, 31, 37). The analysis of disparate streamflow and precipitation records in this region, encompassing much of the headwaters of the Snake and Columbia River basins, highlights a change of substantial magnitude with considerable ecological and economic consequences that has heretofore been ignored or dismissed. At the same time, we note new utility for streamflow data and a potential approach for the assessment of orographic precipitation changes related to increased radiative forcing using macroscale wind information.
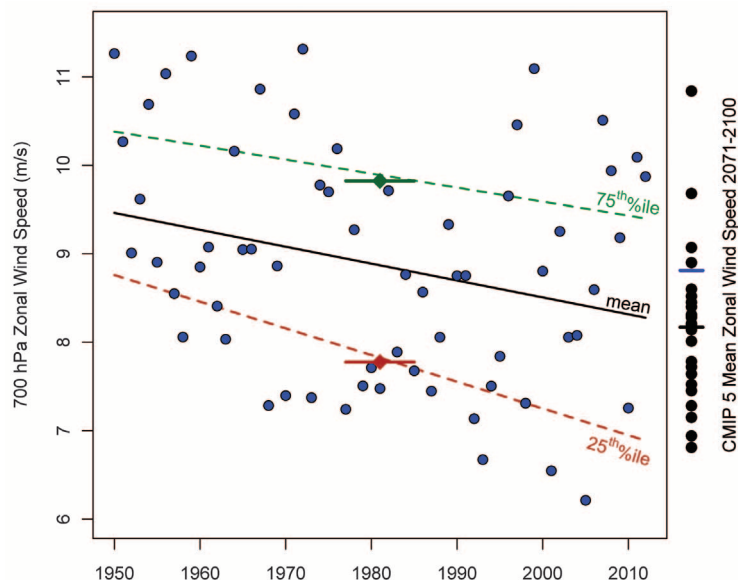


**Fig. 3. Upper-quartile (green), lower-quartile (red), and mean (black) trends in November to March u700 zonal winds averaged over 42.5° to 47.5°N and 115° to 130°W.** Only the mean and lower-quartile trends are significant ($P = 0.03$ and $0.02$, respectively). Also shown with a diamond and bar centered on 1981 are the unconditional quartiles. CMIP5 projections for future wind speeds were calculated from modeled changes between 1950-2005 and 2071-2100 added to the observed 1950–2005 mean (blue bar on right). Estimates for each model are shown as black dots on the right. The mean projection is shown with a black bar.

**Fig. 4. Projected changes in November to March u700 zonal wind averaged across 24 CMIP5 models, 2071–2100 versus 1971–2000 RCP8.5.** Plus signs denote areas where >80% of the models agree on the sign of the change. 20 of the 24 models predict a decrease in the PNW.
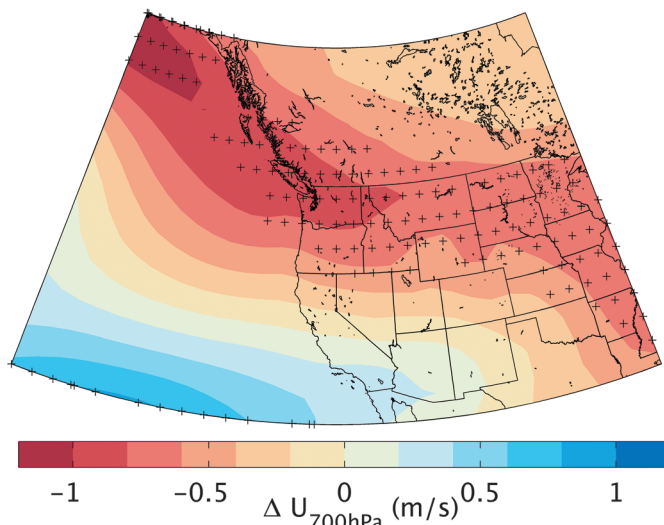
### References and Notes

1. S. Solomon *et al.*, Eds., *Climate Change 2007: The Physical Science Basis. Contribution of Working Group I to the Fourth Assessment, Report of the Intergovernmental Panel on Climate Change* (Cambridge Univ. Press, Cambridge, 2007).
2. P. C. D. Milly *et al.*, *Science* **319**, 573–574 (2008).
3. R. F. Service, *Science* **303**, 1124–1127 (2004).
4. P. W. Mote, A. F. Hamlet, M. P. Clark, D. P. Lettenmaier, *Bull. Am. Meteorol. Soc.* **86**, 39–49 (2005).
5. Z. A. Holden, C. H. Luce, M. A. Crimmins, P. Morgan, *Ecohydrology* **5**, 677–684 (2012).
6. A. E. Cahill *et al.*, *Proc. Biol. Sci.* **280**, 20121890 (2013).
7. S. M. Crimmins, S. Z. Dobrowski, J. A. Greenberg, J. T. Abatzoglou, A. R. Mynsberge, *Science* **331**, 324–327 (2011).
8. T. P. Barnett *et al.*, *Science* **319**, 1080–1083 (2008).
9. S. Regonda, B. Rajagopalan, M. Clark, J. Pitlick, *J. Clim.* **18**, 372–384 (2005).
10. C. H. Luce, Z. A. Holden, *Geophys. Res. Lett.* **36**, L16401 (2009).
11. G. Fu, M. Barber, S. Chen, *Hydrol. Processes* **24**, 866–878 (2010).
12. G. M. Clark, *J. Am. Water Resour. Assoc.* **46**, 486–497 (2010).
13. C. Daly, R. P. Neilson, D. L. Phillips, *J. Appl. Meteorol.* **33**, 140–150 (1994).
14. R. B. Smith, I. Barstad, *J. Atmos. Sci.* **61**, 1377–1391 (2004).
15. B. A. Colle, *J. Atmos. Sci.* **61**, 588–606 (2004).
16. R. B. Smith, in *Advances in Geophysics*, B. Saltzman, Ed. (Academic Press, New York, 1979), vol. 21, pp. 87–230.
17. R. A. Houze Jr., *Rev. Geophys.* **50**, RG1001 (2012).
18. L. Panziera, U. Germann, *Q. J. R. Meteorol. Soc.* **136**, 222–238 (2010).
19. S. E. Yuter, D. A. Stark, J. A. Crouch, M. J. Payne, B. A. Colle, *J. Hydrometeorol.* **12**, 329–351 (2011).
20. M. D. Dettinger, K. T. Redmond, D. R. Cayan, *J. Hydrometeorol.* **5**, 1102–1116 (2004).
21. N. Siler, G. Roe, D. Durran, *J. Hydrometeorol.* **14**, 122–139 (2013).
22. T. P. Burt, N. J. K. Howden, *Water Resour. Res.* **49**, 3504–3515 (2013).
23. M. Hughes, A. Hall, R. G. Fovell, *J. Atmos. Sci.* **66**, 508–518 (2009).
24. Y. Jiang, Y. Luo, Z. Zhao, S. Tao, *Theor. Appl. Climatol.* **99**, 421–430 (2010).
25. T. R. McVicar *et al.*, *Geophys. Res. Lett.* **37**, L06402 (2010).
26. K. Braganza *et al.*, *Clim. Dyn.* **22**, 823–838 (2004).
27. E. R. Cook, C. A. Woodhouse, C. M. Eakin, D. M. Meko, D. W. Stahle, *Science* **306**, 1015–1018 (2004).

28. Z. Gedalof, D. L. Peterson, N. J. Mantua, *J. Am. Water Resour. Assoc.* **40**, 1579–1592 (2004).
29. E. R. Lutz, A. F. Hamlet, J. S. Littell, *Water Resour. Res.* **48**, W01525 (2012).
30. F. M. Ralph *et al.*, *Geophys. Res. Lett.* **33**, L13801 (2006).
31. P. A. O'Gorman, C. J. Muller, *Environ. Res. Lett.* **5**, 025207 (2010).
32. P. C. D. Milly, K. A. Dunne, A. V. Vecchia, *Nature* **438**, 347–350 (2005).
33. E. P. Salathé Jr., L. R. Leung, Y. Qian, Y. Zhang, *Clim. Change* **102**, 51–75 (2010).
34. D. D. Breshears *et al.*, *Proc. Natl. Acad. Sci. U.S.A.* **102**, 15144–15148 (2005).
35. S. J. Wenger *et al.*, *Proc. Natl. Acad. Sci. U.S.A.* **108**, 14175–14180 (2011).
36. G. T. Pederson, J. L. Betancourt, G. J. McCabe, *Geophys. Res. Lett.* **40**, 1811–1816 (2013).
37. J. R. Minder, *J. Clim.* **23**, 2634–2650 (2010).

# Long-Term Dynamics of Adaptation in Asexual Populations

Michael J. Wiser,[1,2] Noah Ribeck,[1,3] Richard E. Lenski[1,2,3]*

Experimental studies of evolution have increased greatly in number in recent years, stimulated by the growing power of genomic tools. However, organismal fitness remains the ultimate metric for interpreting these experiments, and the dynamics of fitness remain poorly understood over long time scales. Here, we examine fitness trajectories for 12 *Escherichia coli* populations during 50,000 generations. Mean fitness appears to increase without bound, consistent with a power law. We also derive this power-law relation theoretically by incorporating clonal interference and diminishing-returns epistasis into a dynamical model of changes in mean fitness over time.

The dynamics of evolving populations are often discussed in terms of movement on an adaptive landscape, where peaks and valleys are states of high and low fitness, respectively. There is considerable interest in the structure of these landscapes (*1–7*). Recent decades have seen tremendous growth in experiments using microbes to address fundamental questions about evolution (*8*), but most have been short in duration. The Long-Term Evolution Experiment (LTEE) with *Escherichia coli* provides the opportunity to characterize the dynamics of adaptive evolution over long periods under constant conditions (*1, 9, 10*). Twelve populations were founded from a common ancestor in 1988 and have been evolving for >50,000 generations, with samples frozen every 500 generations. The frozen bacteria remain viable, and we use this "fossil record" to assess whether fitness continues to increase and to characterize mean fitness trajectories (*11*).
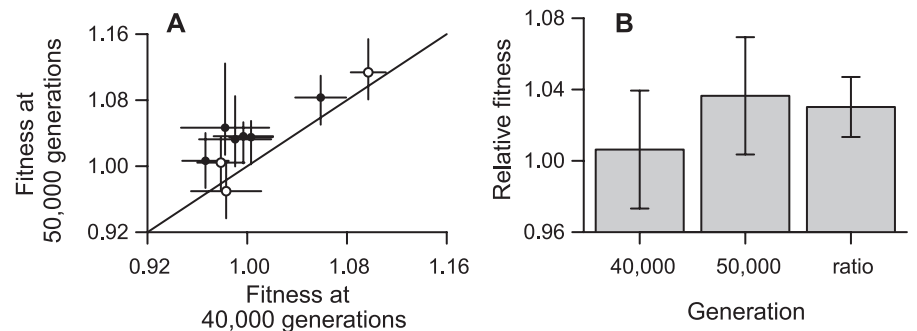
We first performed 108 competitions, in the same conditions as the LTEE, between samples from nine populations at 40,000 and 50,000 generations against marked 40,000-generation clones (*11*). Three populations were excluded for technical reasons (*11*). Fitness was quantified as the dimensionless ratio of the competitors' realized growth rates. Most populations experienced significant improvement (Fig. 1A), and the grand mean fitness increased by 3.0% (Fig. 1B).

To examine the shape of the fitness trajectory, we competed samples from all 12 populations and up to 41 time points against the ancestor (*11*). We compared the fit of two alternative models with the fitness trajectories. The hyperbolic model describes a decelerating trajectory with an asymptote. The power law also decelerates (provided the exponent is <1), but fitness has no upper limit.

Hyperbolic model

$$\overline{w} = 1 + at/(t+b)$$

Power law

$$\overline{w} = (bt+1)^a$$

Mean fitness is $\overline{w}$, time in generations is $t$, and each model has two parameters, $a$ and $b$. Both models are constrained such that the ancestral fitness is 1, hence the offset of +1 in the power law. The hyperbolic model was fit to the first 10,000 generations of the LTEE (*9*), but others suggested an alternative nonasymptotic trajectory (*12*). The grand mean fitness values and the trajectory for each model are shown in Fig. 2A and the individual populations in fig. S1. Both models fit the data very well; the correlation coefficients for the grand means and model trajectories are 0.969 and 0.986 for the hyperbolic and power-law models, respectively. When Bayesian information criterion scores (*11*) are used, the power law outperforms the hyperbolic model with a posterior odds ratio of ~30 million (table S1). The superior performance of the power law also holds when populations are excluded because of incomplete time series or evolved hypermutability (table S1). The power law provides a better fit to the grand-mean fitness than the hyperbolic model in early, middle, and late generations (fig. S2). The power law is supported (odds ratios >10) in six individual populations, whereas none supports the hyperbolic model to that degree (table S2). The power law also predicts fitness gains more accurately than the hyperbolic model. When fit to data for the first 20,000 generations



**Fig. 1. Fitness changes in nine *E. coli* populations between 40,000 and 50,000 generations. (A)** Filled symbols: six populations whose improvement was significant (*P* < 0.05); open symbols: three populations without significant improvement. **(B)** Grand-mean fitness at 40,000 and 50,000 generations relative to 40,000-generation competitor and the ratio of means showing overall gain. Error bars are 95% confidence limits based on replicate assays (A) or populations (B).

[1]BEACON Center for the Study of Evolution in Action, Michigan State University, East Lansing, MI 48824, USA. [2]Department of Zoology, Michigan State University, East Lansing, MI 48824, USA. [3]Department of Microbiology and Molecular Genetics, Michigan State University, East Lansing, MI 48824, USA.

*Corresponding author. E-mail: lenski@msu.edu

Editor's Summary

**Up and Down**

Climate change is expected to have significant impacts on Earth's hydrological cycle, owing to changes, for example, in air temperature, weather patterns, and land surface evaporation. In the Pacific Northwest of the United States, decreases in stream flow have been attributed to increased temperatures. **Luce *et al.*** (p. 1360, published online 29 November) show that these changes in stream flow are not likely to have been caused by temperature change, however, but rather by decreasing precipitation in the mountains where the streams originate.

| | |
|---|---|
| **Article Tools** | Visit the online version of this article to access the personalization and article tools: http://science.sciencemag.org/content/342/6164/1360 |
| **Permissions** | Obtain information about reproducing this article: http://www.sciencemag.org/about/permissions.dtl |